Observations and Numerical Simulation of Atmospheric Cellular Convection over Mesoscale Topography

WENSHOU TIAN AND DOUGLAS J. PARKER

Institute for Atmospheric Science, School of the Environment, University of Leeds, Leeds, United Kingdom

CHARLES A. D. KILBURN

Rutherford Appleton Laboratory, Chilton, Didcot, Oxfordshire, United Kingdom

(Manuscript received 10 December 2001, in final form 26 June 2002)

ABSTRACT

Radar and satellite images provide observations of convective rolls and other structures in the convective boundary layer (CBL), but the data are intermittent, and neither radar nor satellite gives a complete picture of roll circulation in the observed cases. As a consequence, numerical modeling is a useful complement to the observations, to investigate the temporal and spatial details of convective rolls. In this paper, observations of convective rolls over the south of England are described. Numerical simulations have been performed to investigate these rolls using the Boundary Layer Above Stationary Inhomogeneous Uneven Surfaces (BLASIUS) model, a relatively simple boundary layer code for flow over topography. The numerical results indicate that most of the features of the convective structures can be successfully reproduced, notably the roll orientation and spacing and the basic features of the cloud field. These features are in good agreement for two case studies, one with distinct rolls and the other with more dispersed convective structures and a time-dependent basic state. The model tends to predict the initial occurrence of rolls later than observed, and this time of occurrence is found to be influenced by model resolution.

The presence of low topography (with maximum height on the order of 30% of the CBL depth) may have a small influence on the average orientation and spacing, and the time of initial occurrence of modeled rolls. Local flow anomalies related to the hills are much more pronounced. These anomalies appear to be related to coherent patterns in the model cloud fields, with a tendency for more cloud cover upstream and over hills, and cloud clearing in the lee as a result of descent suppressing convective eddies. When the satellite imagery is combined with topography data, this kind of orographic control of the shallow convection by the topography is evident. The CBL height varies considerably in the early stages of CBL evolution over hilly topography, but when the convection is fully developed the CBL height is almost constant over the domain.

1. Introduction

Cellular convection, which takes the form of either two-dimensional rolls or three-dimensional convective cells, is one of the most common forms of atmospheric boundary layer convection. Two-dimensional cells, which are often seen as cloud streets in satellite images, have been known to exist for many decades. However, there are few modeling studies of the phenomenon in the presence of topography.

Kuettner (1959) noted that although individual cumulus streets sometimes originate over and downwind from a heat source, such as an industrial area, a heat island, or a mountain range, the phenomenon in general is independent of orography. Topography tends to disturb rather than create cloud streets and probably for that reason they are best developed over uniform flat terrain and the oceans (Atkinson 1981) and for the same reason they are studied mostly without taking orography into account. Previous studies (e.g., McNider and Pielke 1981; Bader et al. 1987) have simulated the evolving mesoscale boundary layer over complex terrain, but little attention was paid to shallow boundary layer convection (or convective rolls), while numerical simulations of the rolls (e.g., Mason and Sykes 1982; Sykes and Henn 1989; Moeng and Sullivan 1994) were mostly carried out over small domains and flat terrain. Although convective rolls could form and exist over any terrain, orography may modify the formation and evolution of convective rolls by modifying the boundary layer thermodynamic and dynamic conditions, some of which are essential to roll existence. Observations, model simulations, and theoretical analyses have shown that a variety of dynamical factors can affect the roll formation and evolution, and the wind speed, the vertical wind

Corresponding author address: Dr. Douglas J. Parker, Institute for Atmospheric Science, University of Leeds, Leeds LS2 9JT, United Kingdom.
E-mail: doug@env.leeds.ac.uk

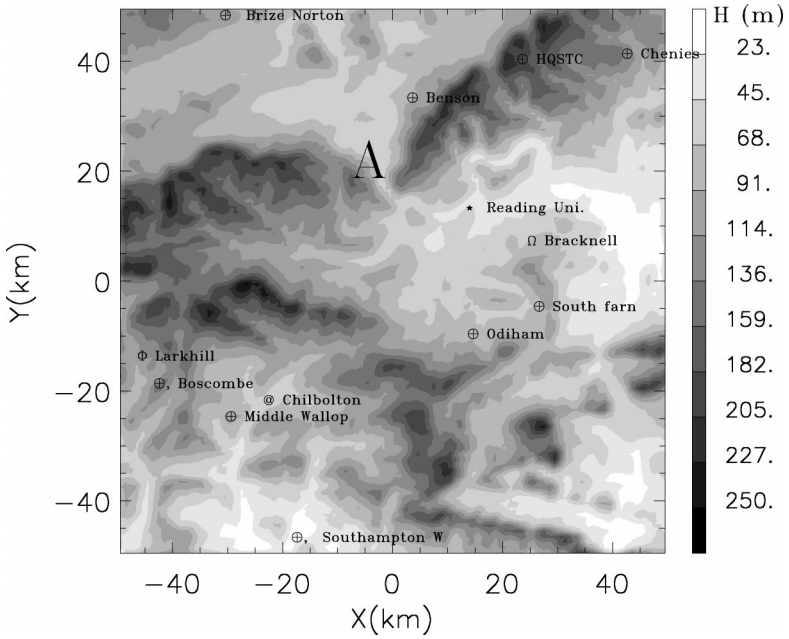

FIG. 1. The topography and the observational network for this study: ⊕ represents synoptic stations, Φ stands for synoptic station with sounding, Ω for the synoptic station with radiation fluxes, ★ for the site with various surface observations including the flux data, and @ represents the Chilbolton radar site. The letter A represents the valley pass.

shear, and the buoyancy, in particular, were thought to be important for the existence of rolls (e.g., Deardorff 1972; LeMone 1973; Moeng and Sullivan 1994; Weckwerth et al. 1997; Khanna and Brasseur 1998; Weckwerth et al. 1999 and references therein). Recently, the observational study by Weckwerth et al. (1999) found that convective rolls can evolve in the absence of significant wind speed and shear, and that the value of wind speed or shear can influence roll evolution, but may not determine when and if rolls would form. Their results suggested that the formation of rolls was dependent on the magnitude of the buoyancy flux, while the decay of rolls was dependent on a convective instability parameter $-z_i/L$, where z_i is the convective boundary layer (CBL) depth and L is the Monin–Obukhov length. The majority of these previous studies have focused on looking for the atmospheric environmental parameters that are responsible for the roll formation and its evolution, without attempts to describe orographic impacts on convective rolls or roll-like convective cells.

In the present work, a numerical model will be used to understand the potential influences of orography on convective rolls and other convective properties through detailed simulation of specific observed cases. Some emphasis will be placed on the model capacity to simulate convective rolls over complex terrain. Section 2 describes the observed cases, section 3 describes the model setup, and section 4 discusses the model results for each case. Section 5 discusses orographic effects in each case and the final section is a summary of the main findings.

2. The dataset and selected observational cases

The topography and the observational network for this study are depicted in Fig. 1. The area is marked by the distinct ridge of the Chilterns, running from the west to the northeast with maximum heights of less than 300 m, and a short valley pass (the Goring Gap, where the River Thames cuts through the Chilterns, marked by the letter A in Fig. 1). The observational data are from various sources including radar images from Chilbolton Observatory, radiosoundings from an upper-air station (Larkhill), surface observations from U.K. Land Surface Stations, and satellite high-resolution visible images from Dundee Satellite Receiving Station.

The Chilbolton Advaned Meteorological Radar (CAMRa) operates at 3 GHz and has 300-m resolution and 60-km range for the observations used in this study. The 25-m antenna of CAMRa gives high sensitivity in a 0.25° beam. The justification for using clear-air radar features to detect convective rolls has been demonstrated by Weckwerth et al. (1997).

In this study, radar images together with satellite images are mainly used to confirm roll existence and to infer roll orientation and wavelength. The satellite data have been superposed on 30″ (approximately 1 km) topographic height data obtained from the Global Land One-kilometer Base Elevation (GLOBE) project. There are 11 U.K. Met Office synoptic stations in the study area. Hourly measurements of the surface wind and the temperature are available from these stations. There is another data source from a field site at Reading Uni-

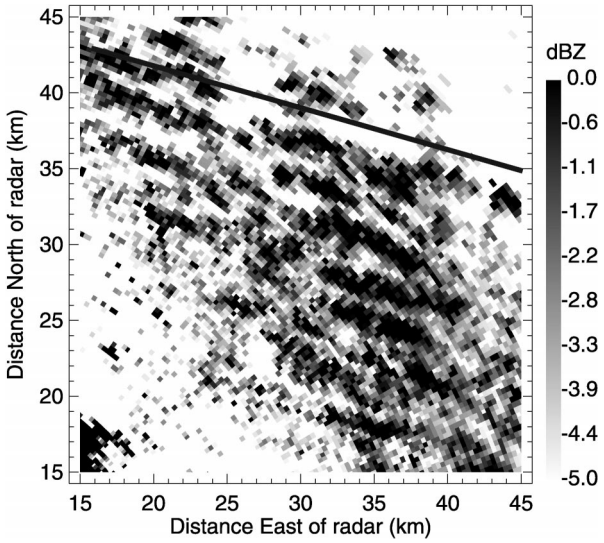

FIG. 2. The radar horizontal scan from Chilbolton at 1000 UTC 12 Aug 1998. The scan elevation is 1°. The heavy dark line (105° from north) represents an estimate of the average roll orientation.

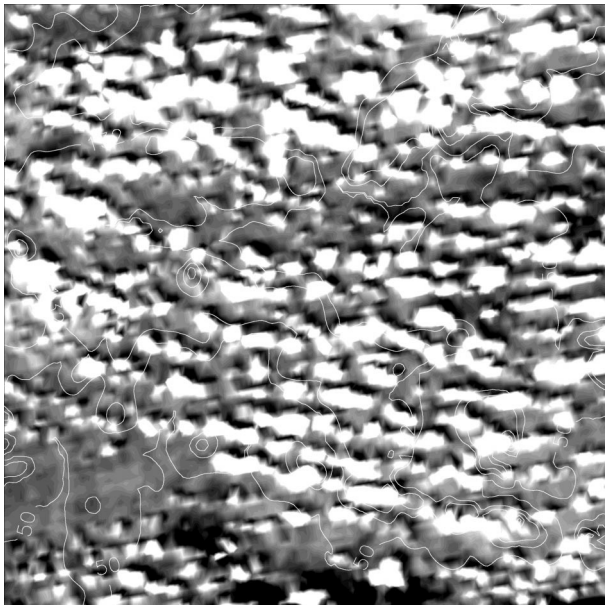

FIG. 4. The high-resolution visible satellite image at 1430 UTC 12 Aug 1998. The underlying topography is represented by the contours. The domain is roughly the same size as that in Fig. 1.

versity where 5-min time series of the surface wind, temperature, humidity, and radiative fluxes are provided by the integral observational system. The sounding and surface observations are used to initialize model runs and to verify model results.

Two observational cases were selected for this study based on the available radar and satellite data, one with well-defined rolls (case 1 on 12 August 1998) and the other with roll-like structures that were less well defined (case 2 on 3 September 1998). The radar imagery for case 1 on 12 August 1998 (Figs. 2 and 3) indicate that roll-like features seem to exist in the early morning at about 1000 UTC. In the satellite imagery, cloud streets are apparent at 1430 UTC (Fig. 4). However, there were no obvious cloud streets in the satellite images before 1430 UTC (not shown) although low clouds were indeed visible over the area. Weckwerth et al. (1997) found that rolls could be observed by radar without the existence of cloud streets in a satellite image. On the other hand, it is interesting that there are no obvious roll-like structures in the radar pictures after 1000 UTC (not shown). The satellite images show a cold front pushing over the United Kingdom during the period from 0600 to 1500 UTC, while the radar images (not shown) indicate that a light shower passed over the study area between 1000 and 1100 UTC. It appears that the shower flushed away

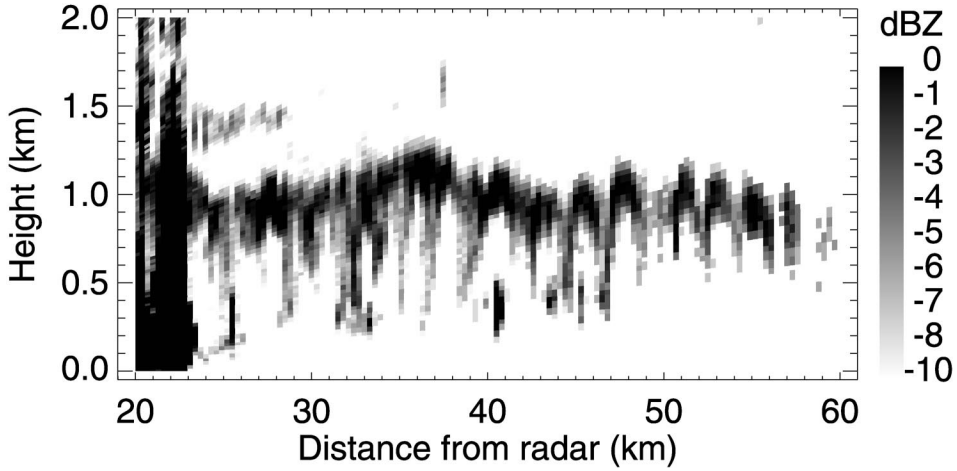

FIG. 3. The radar reflectivity in a vertical plane pointing true north, at 1000 UTC 12 Aug 1998. Note that the upper dark envelope may reflect the CBL top while up and down fluctuations of it may indicate the existence of roll circulation.

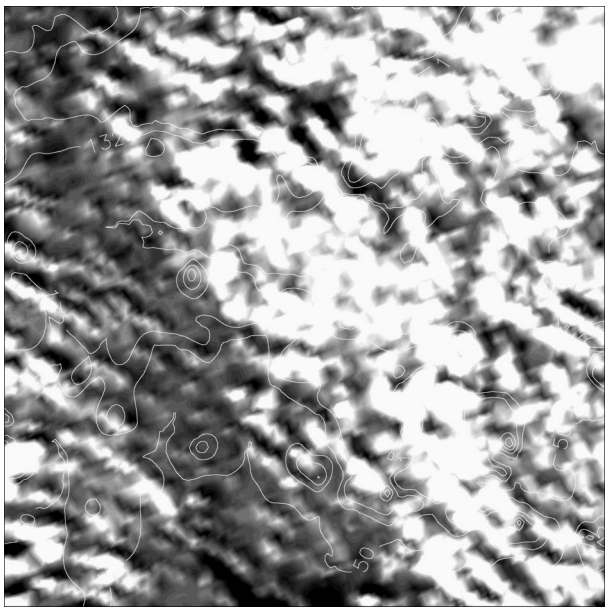

FIG. 5. The high-resolution visible satellite image at 1330 UTC 3 Sep 1998. The domain is the same as in Fig. 4.

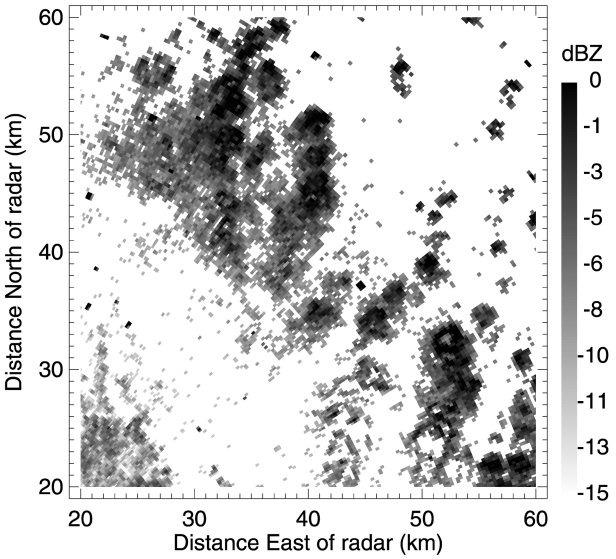

FIG. 6. The radar horizontal scan from Chilbolton at 1103 UTC 3 Sep 1998. The scan elevation is 1°.

the roll structure in the boundary layer, which could be due to the changed refractivity structure in the atmosphere making rolls hard to detect even if they are still present. It should be pointed out that previous observational studies have found that convective rolls could be detected by aircraft photogrammetry after cold air outbreaks or under conditions of postfrontal cold winds (e.g., Kelly 1984). Case 1 shows that although the satellite and radar images each can observe rolls structures, neither is sufficient to determine the presence of these structures under all circumstances.

In case 2 on 3 September 1998, the study area is near the western flank of a cyclone. The low-level clouds exhibited some roll-like structures over the area at 1330 UTC (Fig. 5). The earlier radar image at 1100 UTC (Fig. 6) also suggests that there are some roll-like convective plumes, but the structure is weak and in a different direction to the satellite image structure. Case 2 may represent a transitional case between roll convection and nonroll convection. Both cases selected here are necessary for this study as we are interested to know how the model responds to different convective patterns and orographic forcing under different conditions.

Due to the limited number of images available for these cases, observational description and understanding of the full evolution of convective rolls is not possible. To gain more details of roll evolution and to examine roll features under widely varying environmental conditions, numerical simulation becomes necessary. In the following, the above two cases are studied with the assistance of a numerical model.

3. Numerical model and initialization

The model used is the Met Office boundary layer model Boundary Layer Above Stationary Inhomogeneous Uneven Surfaces (BLASIUS) (e.g., Mason 1987; Wood and Mason 1991). The numerical schemes used in the model are similar to those described by Clark (1977). The turbulence closure scheme is first order and similar to that employed in large eddy simulations (e.g., Deardorff 1974) except that the mixing length scale is arbitrarily chosen. In the scheme, the Reynolds stress terms τ_{ij} and turbulent buoyancy flux H_i (the same for moisture flux) are parameterized as

$$\tau_{ij} = \nu S_{ij} \quad \text{and} \tag{1}$$

$$H_i = \nu \frac{\partial T}{\partial x_i}, \tag{2}$$

where ν is the eddy viscosity and S_{ij} is the deformation tensor defined as

$$S_{ij} = \frac{\partial U_i}{\partial x_j} + \frac{\partial U_j}{\partial x_i} - \frac{2}{3}\delta_{ij}\nabla \cdot \mathbf{U}. \tag{3}$$

In (1) and (2) ν is parameterized as functions of Richardson number Ri, mixing length scale $l(z)$, and wind shear S so that

$$\nu = l(z)^2 S(1 - \mathrm{Ri})^{1/2}, \tag{4}$$

where $S^2 = \frac{1}{2}S_{ij}S_{ij}$, $l(z)$ is defined as

$$\frac{1}{l(z)} = \frac{(1 - \mathrm{Ri})^{1/4}\phi}{\kappa(z + z_0)} + \frac{1}{l_0}, \tag{5}$$

where κ is the von Kármán constant, z_0 is the roughness length, ϕ is the Monin–Obukhov similarity function, and l_0 is a length scale chosen to define the dissipation

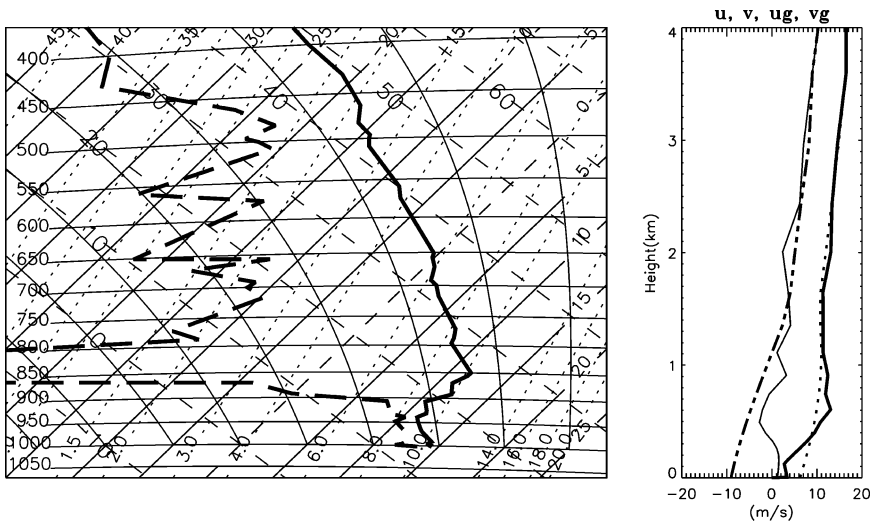

FIG. 7. Initial profiles (0600 UTC) for case 1. The temperature (heavy solid line) and dewpoint temperature (heavy dashed line) profiles are plotted in the tephigram. The heavy solid line in the right panel is for u, the light solid line for v, the dotted line for u_g, and the dashed–dotted line for v_g.

rate. Notice that the eddy viscosities for momentum, buoyancy, and moisture fluxes are assumed to be the same here.

In order to simulate the diurnal evolution of the boundary layer, two major changes are incorporated: 1) the surface temperature T_g and specific humidity are provided by a surface model in which T_g is calculated using a force–restore method as described by Deardorff (1978) and 2) a radiation divergence term is added in the thermodynamic equation. The radiative fluxes and flux divergence are calculated using the emissivity approximation to the radiative transfer equations (e.g., Stephens 1984).

The model was initialized by the radiosonde profiles at 0600 UTC from Larkhill. The surface geostrophic winds u_g and v_g were derived from the pressure observations from four synoptic stations located with in the model domain. At and above 850 hPa, the geostrophic winds are equal to sounding wind profiles while from the surface to 850-hPa level, a linear interpolation was applied. Figure 7 shows the model initial profiles of horizontal velocities u, v and large-scale geostrophic winds u_g and v_g for case 1. For clarity, the temperature and humidity profiles are plotted in the tephigram. The initial profiles are characterized by a significant vertical wind shear and a strong inversion layer around 900 hPa. Note also that the geostrophic wind profile implies a vertical shear in wind direction. The variation of surface geostrophic wind direction with time is not significant from 0600 to 1300 UTC in case 1 (despite the presence of the cold front) and the model profile of geostrophic wind is kept constant in time.

Figure 8 demonstrates the initial conditions for case 2. In contrast to case 1, the atmosphere is only slightly stable but more humid for this case. Both the wind speed and the wind shear are smaller than those in case 1 but the surface geostrophic wind speed is still large. The surface geostrophic wind direction shows an anticyclonic rotation from northerly flow at early morning to nearly westerly in the early afternoon. In the model the geostrophic wind profile is updated hourly, with interpolation between radiosoundings at 0600, 1000, and 1400 UTC. Table 1 gives a summary of the initial background conditions for two cases. It is apparent that the initial conditions and the large-scale flow patterns for case 1 and case 2 are characteristically different from each other with regard to wind shear, wind speed, and thermal stability.

Before discussing the details of roll circulations in the model, it is useful to describe how well the surface temperature is predicted by the surface model as it is crucial to the boundary layer evolution. Figure 9 depicts the diurnal variation of the surface temperature predicted by the model over a uniform surface for case 1 and the observed average surface temperature from 11 synoptic stations. Also shown in Fig. 9 are the surface temperature and the net radiative flux time series from Reading University. A significant temperature drop around 1200 UTC, which was associated with the passage of the cold front, can be noted in the temperature time series at Reading. It is evident that the surface model does a good job although fine details of the temperature variation cannot be resolved. In the initial period of the model simulation, up to around 1130 UTC, the temperature is underestimated compared with observations; the corresponding CBL depth is also lower than that observed by the radar. Large fluctuations in the net radiative flux suggest the presence of clouds. The predicted temperature variation for case 2 is more

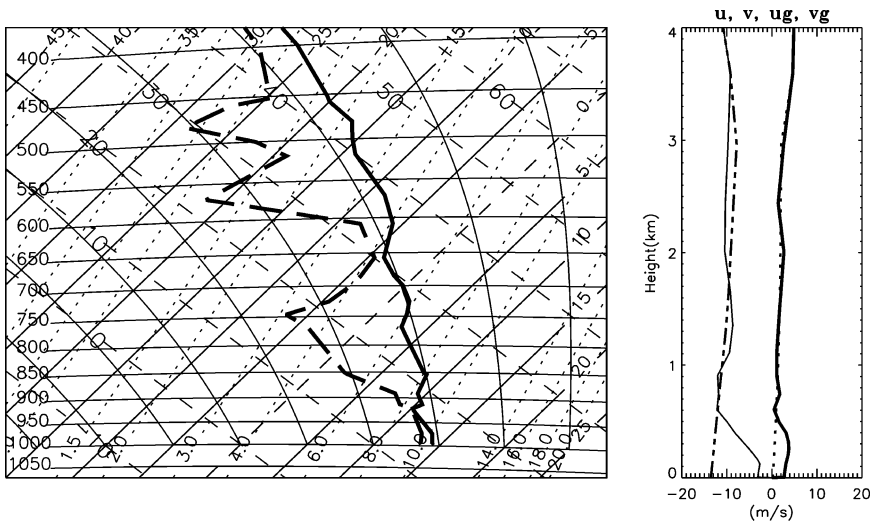

FIG. 8. As in Fig. 7 but for case 2 at 0600 UTC.

consistent with the observations (not shown) because there is no front present.

4. Model results: Roll occurrence and roll morphology

a. Numerical experiments

To detect any material effects of orography on convective rolls, two standard runs will be discussed for each case in this section: a flat terrain run with a 100 km × 100 km horizontal domain will serve as a reference and a run with real orography as shown in Fig. 1 is for detailed study of topographic effects. Random perturbations were added to the initial temperature field to initiate convection in flat terrain runs. A 10-km-deep domain is chosen for all runs and an artificial Rayleigh damping layer is added to the top half of the model domain to minimize reflection.

At the top boundary, the vertical velocity is zero, while zero vertical fluxes are assumed for horizontal wind components. Lateral boundary conditions are periodic. Note that the real terrain with a periodic domain represents a typical topographic spectrum for southern England. The relatively large domain is necessary to represent the larger scales of this spectrum (such as the ridge of the Chilterns). However, it must be remembered in comparing the model results with observations that the upstream topography in the model is not realistic: model features can be regarded as representative of the real atmosphere only if they are produced primarily by local effects.

The model horizontal resolution is 500 m for all standard runs while the vertical mesh is stretched and has 30 points with high vertical resolution near the surface layer. The 500-m horizontal resolution is still coarser than those used in large eddy simulations (LES) of rolls (e.g., Mason and Sykes 1982; Moeng and Sullivan 1994; Weckwerth et al. 1997) but is constrained by computational costs on the mesoscale domain. Based on atmospheric observations, the wavelength of rolls ranges from 0.5 to 4 km (e.g., LeMone 1973; Weckwerth et al. 1999), so a horizontal resolution of 500 m could not resolve the smallest rolls. Here, instead of using high-resolution LES over small flat domain, we are interested in whether convective properties over a relatively large

TABLE 1. The initial background conditions for two cases where U_g is the geostrophic wind speed, U_{gd} is geostrophic wind direction, U_{g0} and U_{gd0} are the surface geostrophic wind speed and direction, T is temperature, Syn is the synoptic setting with Acf representing ahead of cold front, and Nfc representing near flank of cyclone. Gradients have been computed between the surface and 850 hPa. The numbers in parentheses are the corresponding values at 1400 UTC.

Case	U_{g0} (m s^{-1})	U_{gd0} (°)	$-dU_g/dz$ (m s^{-1} km^{-1})	$-dU_{gd}/dz$ (° km^{-1})	$-dT/dz$ (K km^{-1})	Syn
1	11.0	325	0.1	50	1.9	Acf
2	13.5 (8.0)	359 (310)	2.4 (2.0)	6.2 (1.4)	4.5	Nfc

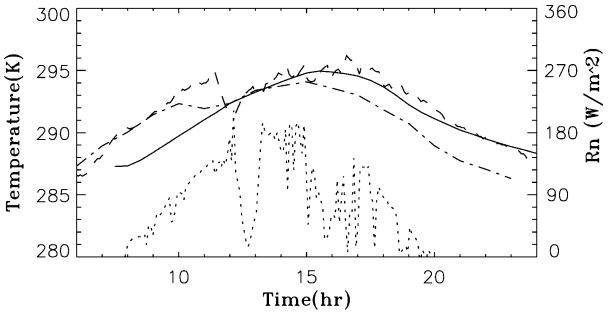

FIG. 9. The predicted and observed diurnal temperature variation. The solid line is the model prediction, the dashed–dotted line is the averaged synoptic observations, the dashed line is the high time resolution observations from Reading. The net radiation flux time series from Reading is also plotted for reference (dotted line).

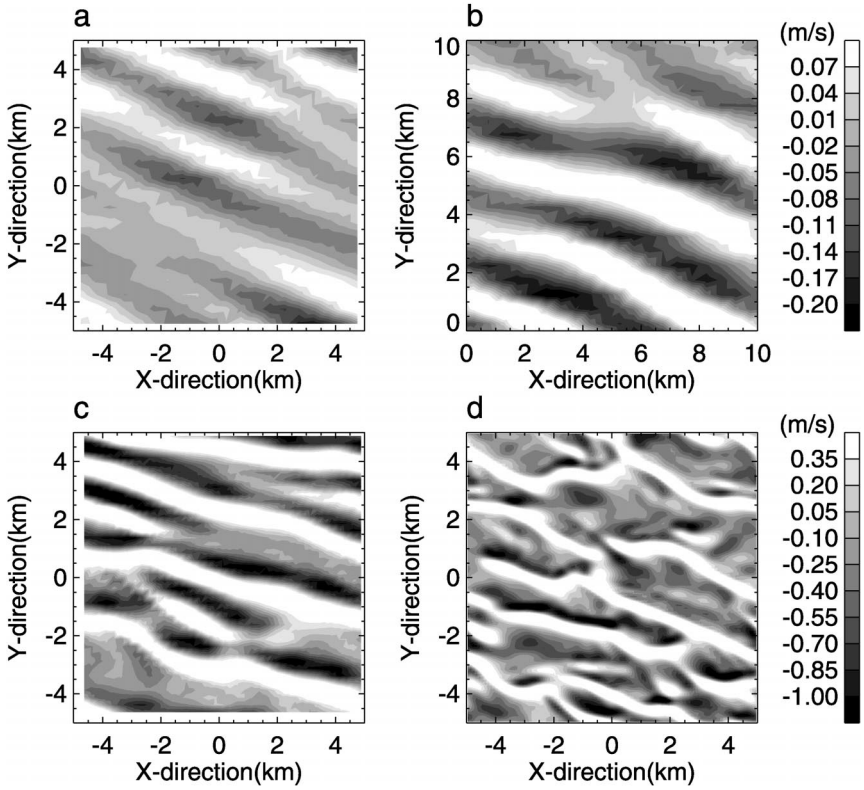

FIG. 10. The instantaneous vertical velocity fields at 150 m AGL gathered at 1100 UTC from four runs: (a) a test run with a 10 km × 10 km horizontal domain and 500-m resolution, (b) the standard flat domain run for case 1 (only results over a 10 km × 10 km region are shown), (c) a test run with a 10 km × 10 km horizontal domain and 250-m resolution, and (d) a test run with a 10 km × 10 km horizontal domain and 100-m resolution. All other model configurations are the same for these runs.

domain with mesoscale topography could be resolved by the model with coarse horizontal resolution and a first-order turbulence scheme.

The model resolution and model domain may affect roll morphology. This issue in two-dimensional cases has been discussed in Tian and Parker (2002). To make our results more definitive, several test runs were performed with different domain sizes and horizontal resolutions. Figure 10 shows instantaneous vertical velocity fields at 150 m above ground level (AGL) gathered from four runs at 1100 UTC: one is the standard flat terrain run for case 1, the other three test runs, which are performed over a 10 km × 10 km domain with different horizontal resolutions, have the same configuration as the standard run. Figure 10 indicates that the domain size has no significant effects on roll characteristics (panels a and b) but the model solution is sensitive to horizontal resolution (panels a, c, and d). The striking difference between these runs is roll occurrence and roll spacing. The corresponding times of roll occurrences in the 100-m, 250-m, 500-m, and 1-km resolution runs are 0930, 1000, 1030, and 1200 UTC, respectively, while the roll spacing in the 1-km resolution test run (3–6 km; not shown) is larger than that in the standard run (2–3 km; Fig. 10b). Those results indicate that a higher horizontal resolution leads to earlier roll occurrence and more fine structure in the rolls. However, the typical roll spacings and orientations are apparently consistent for resolutions of 500 m and finer. It should be pointed out that the differences in the roll spacing implied in Fig. 10 should be interpreted cautiously since the roll circulations set in at different times in these test runs and hence the rolls have evolved for different time periods at 1100 UTC.

Despite the sensitivity of the model solutions to horizontal resolution, it is found that both the mean state and the roll characteristics of orientation and spacing in the 500-m resolution run are close to those in the 100-m resolution run. Although a 500-m horizontal resolution still leads to a 1-h difference in roll occurrence compared with that of a 100-m horizontal resolution, it is an acceptable resolution for the current study as the overall roll properties are resolved. It is also apparent that a 100 km × 100 km domain is large enough to determine roll orientation.

A model parameter of importance is the prescribed mixing length scale l_0 to which the mixing length $l(z)$ is limited though Eq. (5). Choice of l_0 has been dis-

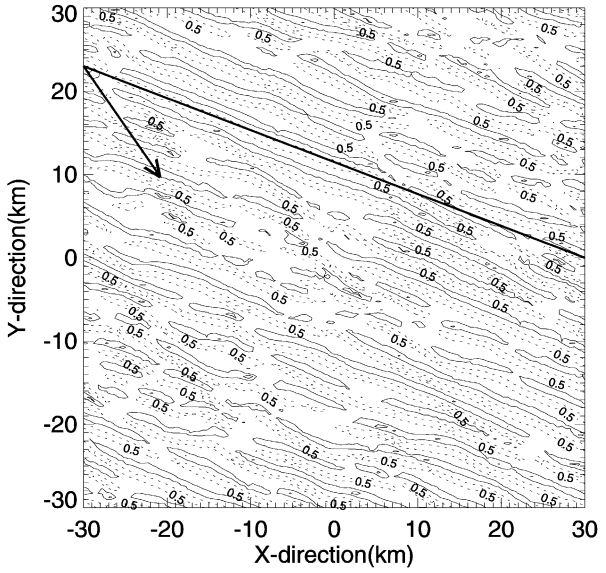

FIG. 11. The instantaneous vertical velocity field at 150 m AGL gathered at 1200 UTC from the standard flat terrain run for case 1. For clarity, only ±0.5 and ±1.0 m s^{-1} contour lines are drawn. The average roll orientation (111°) is represented by the heavy dark line. The surface geostrophic wind direction (325°) is given by the arrow.

cussed in detail by Mason and Sykes (1980, 1982). They found that the stability of the model solutions obtained by the above mixing length scheme is affected by the choice of l_0, and that horizontal grid length modes may build up slowly near the surface layer in simulations undertaken with this turbulence scheme while increasing the horizontal resolution only slightly reduces them. According to Mason and Sykes (1980), the data of LeMone (1973) suggest the magnitude of l_0 to be about 40 m. However, our test runs indicate that 40 m is not a good choice of l_0 for both cases. For case 1, the model solution with $l_0 = 40$ m lost stability after 5 h even over flat domain and no rolls can be generated except grid-scale modes. For case 2, although the physical property of the solution with $l_0 = 40$ m is retained over flat terrain, the solution over hilly terrain lost stability quickly. An appropriate value of l_0 for both cases is found to be 100 m. It should be pointed out that there is no simple, general justification for any particular value of l_0. In convective circumstances l_0 is found to be related to the CBL depth and the deeper the CBL, the larger l_0 should be. Further tests indicate that l_0 has little effect on the occurrence of rolls although it has a large impact on the eddy energy and eddy growth rate. A large l_0 tends to suppress or diffuse resolved rolls. The selection of an appropriate l_0 depends on the case under consideration and, in particular, depends on the near-surface wind field and thermal stability.

b. Case 1

Figure 11 shows the instantaneous vertical velocity field at 150 m AGL gathered at 1200 UTC from the standard flat terrain run. For clarity, only the results over a 60 km by 60 km inner region of the model domain are shown. Line convective structures are fully developed from 1200 UTC onward. Weak resolved roll signals can be noted at 1030 UTC (not shown) and well-defined rolls begin to appear at 1100 UTC (Fig. 10b). The predicted roll occurrence is about 30 min later than observed in Fig. 2. The roll axis in Fig. 11 is aligned 111° ± 5° from north (with the angle and errors estimated by hand from the figures), which is about 34° to the left of the near-surface geostrophic wind direction. This relatively large angle is probably due to the veering of the geostrophic wind with height.

A roll wavelength of around 2–3 km is inferred from Fig. 11. The model temperature field at 1200 UTC (not shown) suggests that the CBL depth is about 800 m. The results here imply aspect ratios (ratio of roll wavelength to CBL depth) of 2.5–3.8. The radar-observed CBL depth (Fig. 3) is about 1 km at about 1000 UTC and the roll wavelength is about 2–4 km (Fig. 2), and as a result, the observed aspect ratios are about 1.6–3.3, which are consistent with the predicted values. Both predicted and observed aspect ratios are within the range of the previous findings (LeMone 1973; Weckwerth et al. 1997).

Figure 12 displays the instantaneous vertical velocity fields at 150 m AGL gathered at 1030 UTC from the real-terrain run. Consistent with the results from the flat-terrain run, resolved convective rolls begin to be apparent over relatively flat areas at 1030 UTC with an orientation of about 102° ±5°. The rolls are fully developed over the domain at 1200 UTC (Fig. 13), and roll orientation is around 105° ±5°, about 6° less than that over the flat domain. The predicted orientations over flat domain and over real terrain are close to the observed value, which is approximately 105° ±5° in Fig. 2. The aspect ratios are overall the same as those over flat terrain. Although rolls over real terrain are stronger than those over the flat domain at the time when line structures begin to appear, the time of roll occurrence is not significantly (within 30 min) affected by the structure and character of the perturbations, whether random-noise or terrain-induced perturbations. We can also note from Fig. 13 that the fully developed rolls are only slightly disturbed by orography as the orography is well within the CBL and the rolls are strong.

c. Case 2

For case 2, a slice of the vertical velocity field at 1100 UTC from the standard flat-terrain run at 150 m. AGL is displayed in Fig. 14. The convective activity is sporadic and not organized at 1100 UTC. This may suggest that the convective structure in Fig. 6 is made up of convective plumes rather than rolls. At 1200 UTC, convective eddies become more like rolls (not shown) and become more organized at 1230 UTC (Fig. 15). The rolls are not as regular as those in case 1, with some of

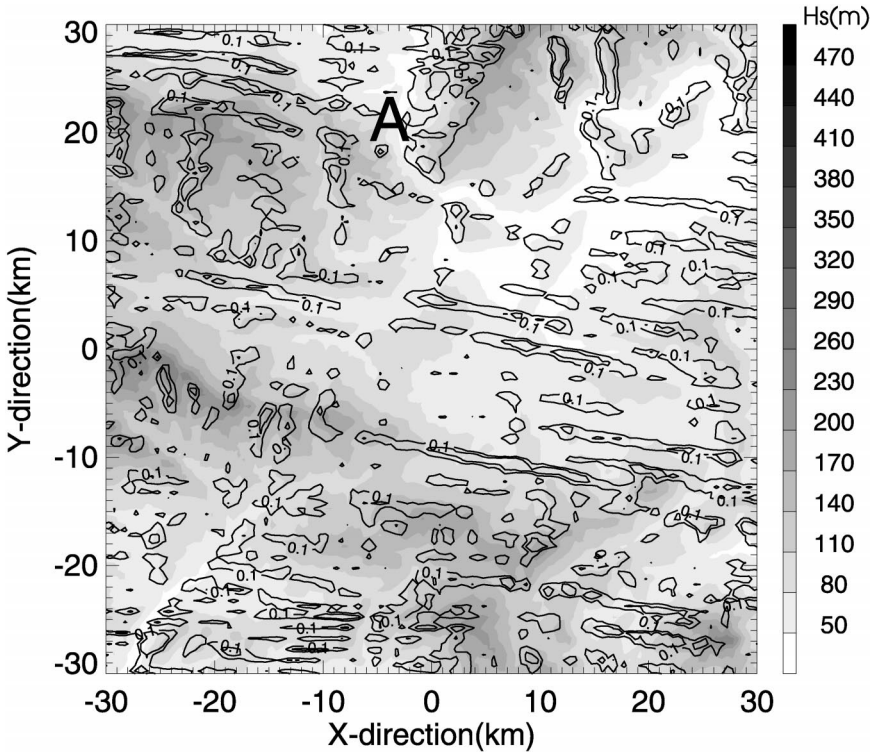

FIG. 12. The instantaneous vertical velocity field at 150 m AGL gathered at 1030 UTC, from the real-terrain run for case 1. Only 0.1 and 0.3 m s^{-1} contour lines are drawn for the vertical velocity field for clarity. The background shading represents topography.

them being vigorous but discontinuous and tending to bifurcate, while others are weak and tending to break or be absorbed by others. An approximate orientation of 138° ±5° can be detected that is, overall, the same as observed in Fig. 5. This orientation of the rolls at 1230 UTC is about 7° to the left of the near-surface geostrophic wind direction (similar to Angell et al. 1968). Note that the convective structures at 1100 and 1230 UTC are quite different. Using a time-dependent geostrophic wind profile in the model successfully resolves this variation in eddy alignment. Apparently, the roll characteristics respond rapidly to the changing geostrophic state.

Figure 16 shows a horizontal slice of instantaneous vertical velocity at 150 m AGL gathered from the real-terrain run at 1230 UTC. The line structures are quite evident over real terrain. The rolls are more steady than those over the flat domain and rather linearly aligned. The roll orientation is also about 138° ±5°, which is nearly the same as that over flat domain, and roll spacing ranges from 1 to 3 km. It should be pointed out that numerical noise becomes evident on the grid scale near the surface layer after a period of simulation in both cases. However, the noise imposes no significant influences on overall convective structures and their evolution.

Again, the results here suggest that the occurrence of rolls is not too different between these over real terrain and flat domain. It is hard to compare the roll aspect ratios between observations and the model results for this case as the roll circulations are not as pronounced in the radar image. However, the qualitative characteristics of intermittent and broken circulations are consistent between observations and model results.

The general features of convective rolls have been successfully simulated in the presence of real orography. The main differences between model results and observations lie in the timing of roll occurrence and in roll wavelength. Numerically, these differences appear to be caused mainly by model horizontal resolution.

5. Orographic effects on convective properties

a. Orientation and spacing of rolls

We have noted in the simulations with respect to case 1 that the orography seems to have an impact on the orientation of the rolls (approximately 6° ±5° difference between the orientation over the flat terrain and that over real terrain), and the simulations associated with case 2 suggest insignificant orographic effects on the roll orientation.

Previous studies have proposed various dynamic instabilities, such as shear instability (e.g., Kelly 1984) and Ekman-layer inflection point instability (Brown 1972), to predict roll orientation. Although different ref-

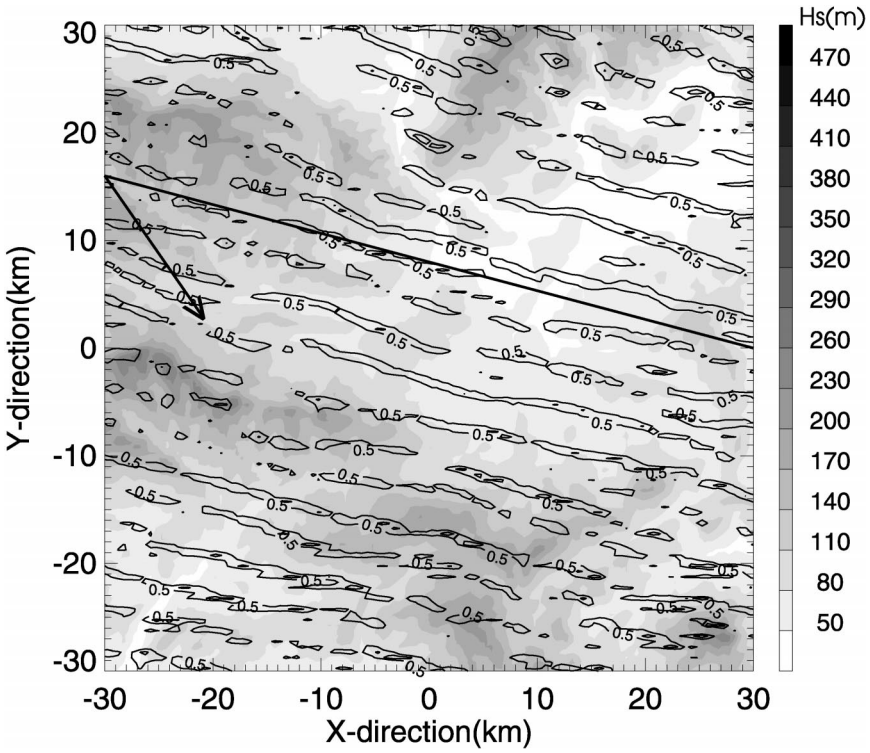

FIG. 13. As in Fig. 12 but at 1200 UTC and for contour lines that are 0.5 and 1.0 m s^{-1}. The average roll orientation (105°, the heavy dark line) and the surface geostrophic wind direction (325°, the arrow) are also given.

erence wind vectors such as the roll-layer wind (Kuettner 1971), surface wind vector (Deardorff 1972), and the geostrophic wind vector (Brown 1972), have been used in their prediction, their results all suggested that roll orientation is highly related to low-level wind and wind shear. Here, it is found that a difference of 3° in the low-level horizontally averaged wind direction can be noted between the flat- and real-terrain simulations in case 1 (with nearly unchanged average wind speed), while in case 2 this difference is insignificant. Also, in case 1 the modeled roll orientation is much more spatially variable than that in case 2.

It is also possible that the orientation of rolls is modified by an interaction with gravity waves. Inspection of the gravity wave patterns in the model for case 1 at 0900 UTC (not shown) indicates an approximate north–south orientation to these waves, and it is hard to infer a mechanism for coupling with rolls. If the alignment of gravity wave phase lines is close to the roll orientation, the interaction between rolls and waves suggested by Clark et al. (1986) is more likely to exist and to increase the roll spacing. If there is a wide angle between the roll orientation and the wave alignment (as we have inferred for case 1), then the waves may only disturb the roll intensity rather than increase the roll spacing. For case 2, a comparison of Figs. 15 and 16 reveals that orography has an impact on the organization of the rolls as one can note that the roll circulations are more organized more uniformly, with more regular and wider separation over real terrain than those over flat domain.

It appears that the local orographic effects on roll circulation are more pronounced in case 1 that in case 2. Rolls are significantly disturbed over elevated regions in case 1 in the early stage of the rolls (Fig. 12), and an approximate 6° ±5° difference in roll orientation can be detected between those over the flat domain and the real terrain. The roll circulations in case 2 are quite vigorous, and as a result, the orographic signature on them is less evident. However, in this case significant effects on the organization and spacing of rolls can be noted.

b. Cloud formation and CBL depth

In terms of orographic effects on convection, we are also interested in the orographic triggering of moist convection under favorable conditions. Wilson et al. (1992) have given an observational case in which horizontal rolls and the orogenic convergence line together were found to have contributed to initializing a deep storm. Whether rolls alone can initialize deep convection is still open to question, but orography may adjust roll orientation, spacing, and local intensity sufficiently to initiate moist convection.

In theory any terrain-generated vertical motions may

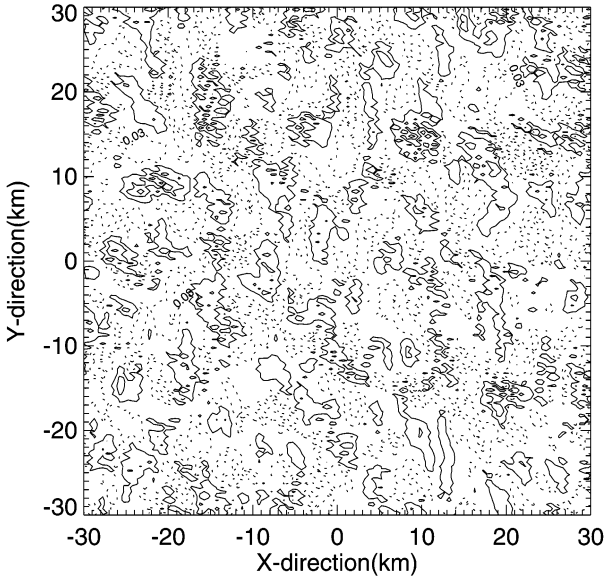

FIG. 14. The instantaneous vertical velocity field at 150 m AGL at 1100 UTC from the standard flat-terrain run for case 2. The contour lines are ± 0.05 and ± 0.1 m s^{-1}.

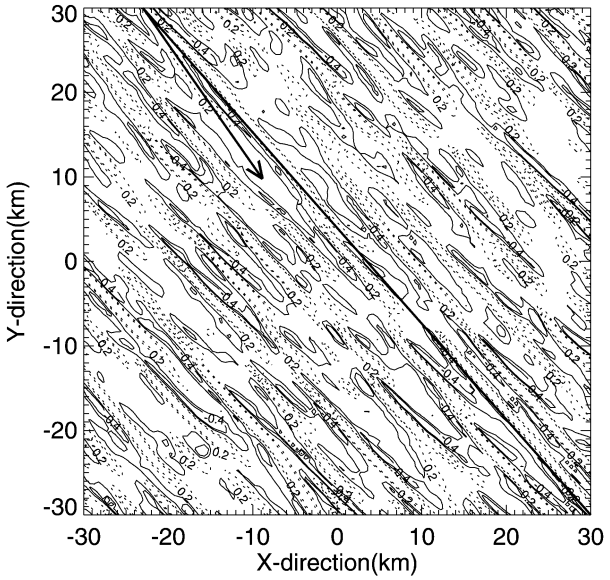

FIG. 15. As in Fig. 14 but at 1230 UTC. The contour lines are ± 0.2 and ± 0.4 m s^{-1}. The average roll orientation (138°) is represented by the heavy dark line. The arrow stands for the surface geostrophic wind direction.

have impacts on the convective activity. Apart from convective rolls and the terrain-induced gravity waves, another kind of terrain-induced vertical motion that may have potential to trigger deep convective systems can be detected in Figs. 12 and 17. The persistent vertical motion at low levels north and upwind of the Goring Gap (marked A in Figs. 12 and 17) is mechanically forced by orography. Significant forced ascents and descents, which may enhance smaller-scale convective updrafts at the windward slope of orography and suppress convective clouds in the lee, can also be detected over elevated regions, for example, in the southeast of the domain. Tian and Parker (2002) have discussed this argument in detail based on idealized simulations.

To provide further evidence about this kind of orographic effect, the relative humidity fields from two real-terrain simulations are diagnosed (note that there are no cloud microphysical processes resolved in the model). The time-averaged column maximum relative humidity field (using half-hourly realizations from 0630 to 1300 UTC), which roughly represents the average cloud cover, is depicted for both cases in Fig. 18. It is apparent that the hilly areas and windward slopes of higher ridges are marked by more clouds, and there are relatively less clouds in the lee of these ridges such as the Chilterns. Recall that in case 2 the orientation of convective eddies has changed significantly during this period.

Observational confirmation of this pattern can be found in Fig. 4. The satellite imagery shows enhanced roll clouds upwind and over the Chilterns and a suppression of roll convection in the lee of the Chilterns. Dynamically we can attribute the suppression of eddies in the lee of hills to descent of the mean wind; because of the relatively low orography and high geostrophic winds in both cases, the thermally direct circulation forced by the heated terrain is not pronounced (as quantified by Tian and Parker 2002).

Another interesting point is the CBL depth over hilly terrain, which is an important indicator in orographic triggering of convection. Model results seem to suggest that CBL depths over hilly terrain are not so different from those over flat terrain when convection is fully developed, for example, at 1200 UTC in case 1. However, Fig. 19 indicates that orographic effects on the CBL depth and cloud formation are pronounced in the earlier stages of the CBL evolution. The CBL depth is different over different regions of the domain (Fig. 19a). Figure 3 also shows that the CBL depth has a significant variation in the horizontal. These structures are partly influenced by an interaction with gravity waves above the CBL and are therefore not easily diagnosed ''by eye'' in the 3D domain. However, the terrain-induced cloud formation can be inferred in Fig. 19b and agrees qualitatively with observations.

6. Summary and remarks

Convective rolls over orography have been studied through numerical modeling combined with radar and satellite observations from two case studies. The observations provide good details about roll orientation and wavelength, but neither radar nor satellite data alone are sufficient to fully characterize the time evolution for these cases. The visible satellite data are an efficient means for detecting orographic control of these shallow convective structures, when topography is superposed. Ongoing study is currently attempting to use other mea-

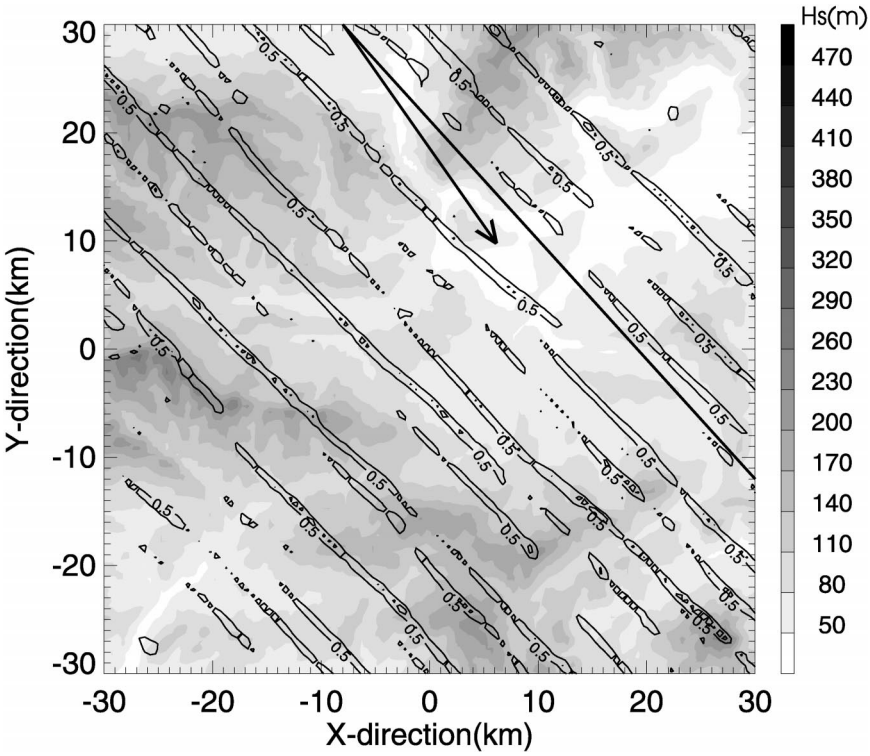

FIG. 16. The instantaneous vertical velocity field at 150 m AGL at 1230 UTC from the real-terrain run for case 2. The contour lines are 0.5 and 1.0 m s^{-1} for vertical velocity. The heavy dark line and the arrow represent the average roll orientation (138°) and the surface geostrophic wind direction (325°), respectively.

surements to detect roll structure, including microbarograph data at the surface and a cloud lidar.

The model-predicted roll characteristics are generally consistent with the observations although the predicted time of the roll occurrence is later than that of the radar observations, apparently because of the relatively course model resolution used. The simulations with respect to both observational cases suggest that the time of the roll occurrence is not significantly affected by the character of the perturbations, and that orography initiates convective rolls only slightly earlier (within 30 min) than random perturbations do.

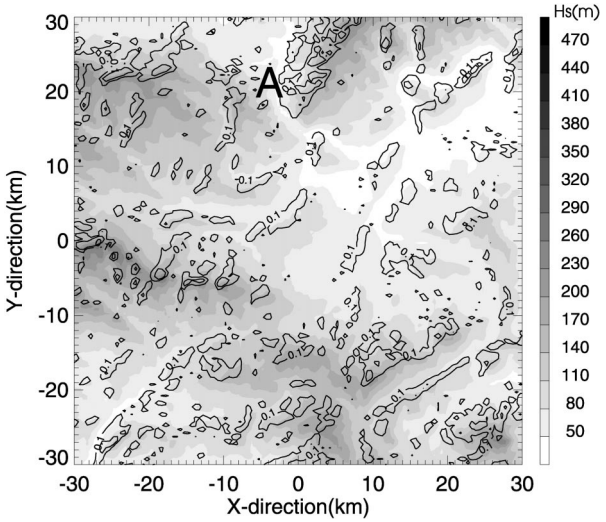

FIG. 17. As in Fig. 16 but at 1100 UTC. The contour lines are 0.1 and 0.3 m s^{-1} for vertical velocity.

Once formed, the characteristics of rolls such as orientation and spacing are slightly modified by terrain-induced flows, and the degree of modification varies between cases over the same terrain. However, the model results suggest that forced ascent caused by orography and the corresponding descent have significant impacts on the convective activity and the resulting cloud field. Strong evidence of this can be detected from a satellite image and model simulations. The top of the CBL can vary significantly over a hilly domain at the initial stage of CBL evolution, while persistent upward motions around a valley pass (the Goring Gap) are particularly noticeable.

Certain key factors affect the model results in simulating the convective rolls. The limiting mixing length, l_0, has a significant impact on the model simulation and the appropriate l_0 is often varied from one observational case to another. It is apparent that it is not ideal to prescribe a l_0 in long time simulations with the current

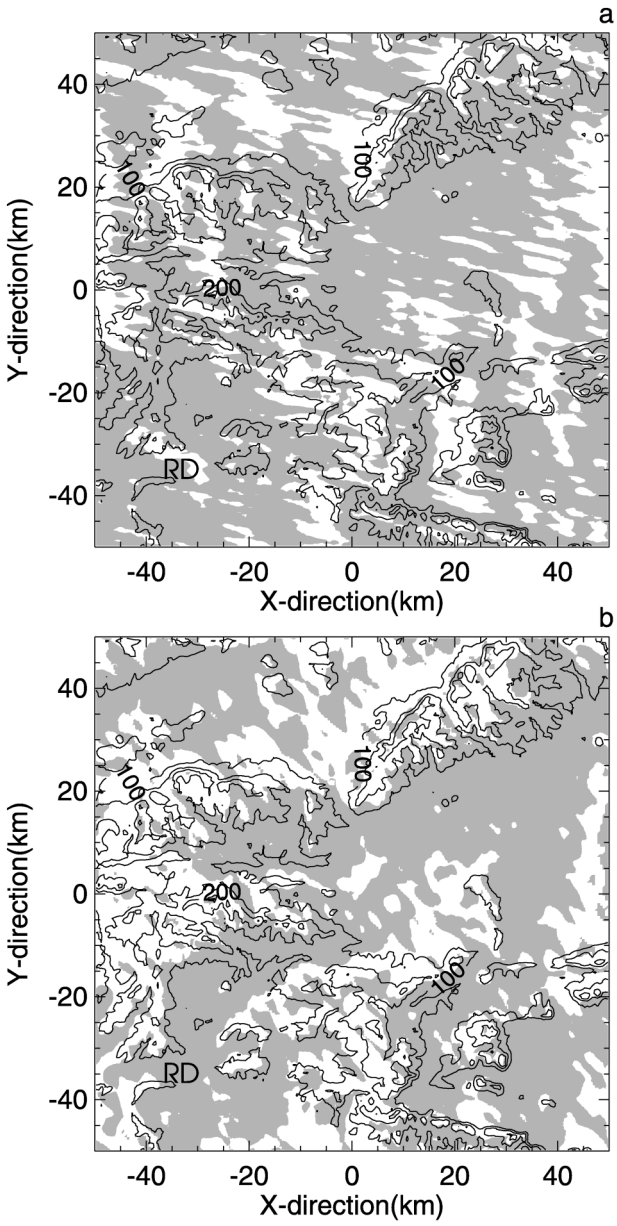

FIG. 18. The time-averaged (from 0630 to 1300 UTC) column maximum relative humidity field diagnosed for (a) case 1, in which mean relative humidity less than 92% is shaded, and (b) case 2, shaded for relative humidity less than 99%. The terrain is represented by contours.

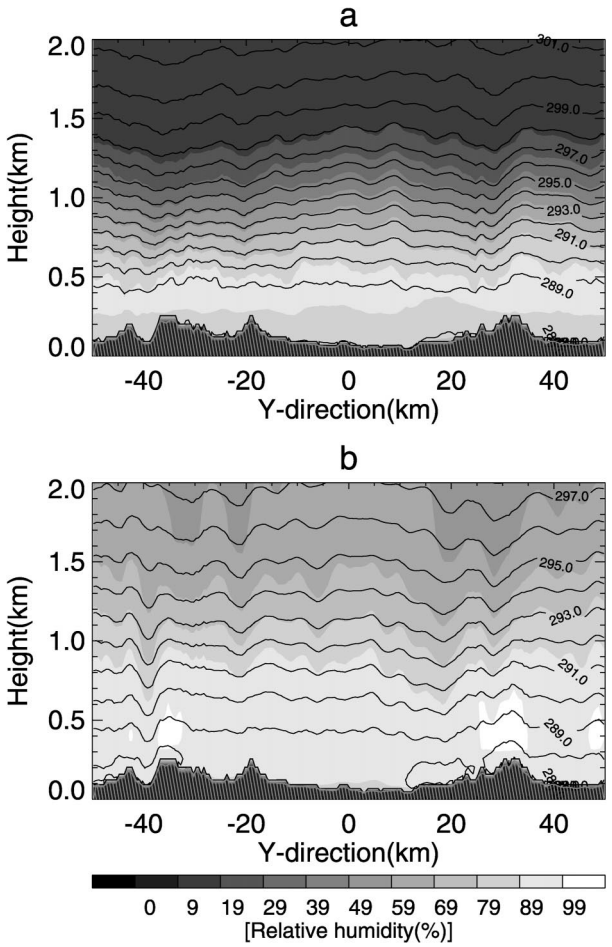

FIG. 19. The *y*–*z* cross sections, at $x = 10$ km in Fig. 1, of the instantaneous potential temperature fields gathered at 0900 UTC from the real-terrain run with respect to (a) case 1 and (b) case 2 (contour lines). The corresponding relative humidity fields are superposed for reference (shaded).

model and an improvement in determining l_0 is necessary unless another turbulence scheme is to be adopted. The simulation of convective rolls is also hampered by the difficulty of providing the model with a time-dependent geostrophic wind profile, so relatively frequent soundings are necessary. However, the model results shown here demonstrate that many of the details of the evolution and structure of convective eddies can successfully be simulated in a relatively simple numerical model. Overall we can see that the orography typical of southern England does control local convective structure and cumulus formation and that the prospects are good for model skill in reproducing these observations. There may be opportunities for finescale forecasting of local convective flows within the coming years.

Acknowledgments. Wenshou Tian has been supported by an Overseas Research Scholarship. Flux data from the University of Reading were kindly provided by Dr. Giles Harrison and Mr. Andrew Lomas. Dr. Chang Gui Wang of the JCMM gave assistance in processing the satellite data, which were provided by NERC Satellite Receiving Station, Dundee University, Scotland (http://www.sat.dundee.ac.uk/). Radar data were taken for the Met Office DROP project and thanks are due to Prof. Paul Hardaker and Mr. Andrew Pilditch for discussions on radar data analysis. Topographic data were supplied by the GLOBE project (http://www.ngdc.noaa.gov/seg/topo/globedoc.shtml). Synoptic and radiosonde data were obtained from the British Atmospheric Data Centre

(BADC). Comments from two anonymous reviewers have improved the clarity of the results.

REFERENCES

Angell, J. K., O. M. Pack, and C. R. Dickson, 1968: A Lagrangian study of helical circulations in the planetary boundary layer. *J. Atmos. Sci.,* **25,** 707–717.

Atkinson, B. W., 1981: *Meso-scale Atmospheric Circulation.* Academic Press, 488 pp.

Bader, D. C., T. B. McKee, and G. J. Tripoli, 1987: Mesoscale boundary layer evolution over complex terrain. Part I: Numerical simulation of the diurnal cycle. *J. Atmos. Sci.,* **44,** 2823–2838.

Brown, R. A., 1972: On the inflection point instability of a stratified Ekman boundary layer. *J. Atmos. Sci.,* **29,** 850–859.

Clark, T. L., 1977: A small-scale dynamic model using a terrain-following transformation. *J. Comput. Phys.,* **24,** 186–215.

——, T. Hauf, and J. P. Kuettner, 1986: Convectively forced internal gravity waves: Results from two-dimensional numerical experiments. *Quart. J. Roy. Meteor. Soc.,* **112,** 899–925.

Deardorff, J. W., 1972: Numerical investigations of neutral and unstable boundary layers. *J. Atmos. Sci.,* **29,** 91–115.

——, 1974: Three-dimensional numerical study of the height and mean structure of the heated planetary boundary layer. *Bound.-Layer Meteor.,* **7,** 81–105.

——, 1978: Efficient prediction of ground-surface temperature and moisture, with inclusion of a layer of vegetation. *J. Geophys. Res.,* **83,** 1889–1903.

Kelly, R. D., 1984: Horizontal roll and boundary-layer interrelationship observed over Lake Michigan. *J. Atmos. Sci.,* **41,** 1816–1826.

Khanna, S., and J. G. Brasseur, 1998: Three-dimensional buoyancy and shear-induced local structure of the atmospheric boundary layer. *J. Atmos. Sci.,* **55,** 710–743.

Kuettner, J., 1959: The band structure of the atmosphere. *Tellus,* **11,** 267–294.

——, 1971: Cloud bands in the earth's atmosphere—Observations and theory. *Tellus,* **23,** 404–425.

LeMone, M. A., 1973: The structure and dynamics of horizontal roll vortices in the planetary boundary layer. *J. Atmos. Sci.,* **30,** 1077–1091.

Mason, P. J., 1987: Diurnal variations in flow over a succession of ridges and valleys. *Quart. J. Roy. Meteor. Soc.,* **113,** 1117–1140.

——, and R. I. Sykes, 1980: A two-dimensional numerical study of horizontal roll vortices in the neutral atmospheric boundary layer. *Quart. J. Roy. Meteor. Soc.,* **106,** 351–366.

——, and ——, 1982: A two-dimensional numerical study of horizontal roll vortices in an inversion capped planetary boundary layer. *Quart. J. Roy. Meteor. Soc.,* **108,** 801–823.

McNider, R. T., and R. A. Pielke, 1981: Diurnal boundary-layer development over sloping terrain. *J. Atmos. Sci.,* **38,** 2198–2212.

Moeng, C. H., and P. P. Sullivan, 1994: A comparison of shear and buoyancy driven planetary boundary layer flows. *J. Atmos. Sci.,* **51,** 999–1022.

Stephens, G. L., 1984: The parameterization of radiation for numerical weather prediction and climate models. *Mon. Wea. Rev.,* **112,** 826–867.

Sykes, R. I., and D. S. Henn, 1989: Large-eddy simulation of turbulent sheared convection. *J. Atmos. Sci.,* **46,** 1106–1118.

Tian, W.-S., and D. J. Parker, 2002: Two-dimensional simulation of orographic effects on mesoscale boundary layer convection. *Quart. J. Roy. Meteor. Soc.,* **128,** 1929–1952.

Weckwerth, T. M., J. W. Wilson, R. M. Wakimoto, and N. A. Crook, 1997: Horizontal convective rolls: Determining the environmental conditions supporting their existence and characteristics. *Mon. Wea. Rev.,* **125,** 505–526.

——, T. W. Horst, and J. W. Wilson, 1999: An observational study of the evolution of horizontal convective rolls. *Mon. Wea. Rev.,* **127,** 2160–2179.

Wilson, J. W., G. B. Foote, N. A. Crook, J. C. Fankhauser, C. G. Wade, J. D. Tuttle, and C. K. Mueller, 1992: The role of boundary-layer convergence zones and horizontal rolls in the initiation of thunderstorms: A case study. *Mon. Wea. Rev.,* **120,** 1785–1815.

Wood, N., and P. Mason, 1991: The influence of static stability on the effective roughness length for momentum and heat transfer. *Quart. J. Roy. Meteor. Soc.,* **117,** 1025–1056.